When architectural plasticity fails to counter the light competition imposed by planting design: an in silico approach using a functional–structural model of oil palm

Raphael P. A. Perez, Rémi Vezy, Loïc Brancheriau, Frédéric Boudon, François Grand, Merlin Ramel, Doni Artanto Raharjo, Jean-Pierre Caliman, Jean Dauzat

in silico Plants Vol. 4, No. 1, pp. 1–16
https://doi.org/10.1093/insilicoplants/diac009
Advance Access publication 26 May 2022
Special Issue: Functional–Structural Plant Models
Original Research

in silico Plants
OXFORD

When architectural plasticity fails to counter the light competition imposed by planting design: an *in silico* approach using a functional–structural model of oil palm

Raphaël P. A. Perez[1,2,*], Rémi Vezy[3,4], Loïc Brancheriau[5,6], Frédéric Boudon[1,2], François Grand[3,4], Merlin Ramel[3,4], Doni Artanto Raharjo[7], Jean-Pierre Caliman[7] and Jean Dauzat[3,4]

[1]CIRAD, UMR AGAP Institut, F-34398 Montpellier, France
[2]UMR AGAP Institut, Univ Montpellier, CIRAD, INRAE, Institut Agro, F-34398 Montpellier, France
[3]CIRAD, UMR AMAP, F-34398 Montpellier, France
[4]AMAP, Univ. Montpellier, CIRAD, CNRS, INRAE, IRD, F-34398 Montpellier, France
[5]CIRAD, UPR BioWooEB, F-34398 Montpellier, France
[6]BioWooEB, Univ. Montpellier, CIRAD, CNRS, INRAE, IRD, F-34398 Montpellier, France
[7]Sinar Mas Agro Resources Technology Research Institute (SMARTRI), Pekanbaru, Indonesia
*Corresponding author's e-mail address: raphael.perez@cirad.fr

Guest Editor: Katrin Kahlen
Editor-in-Chief: Stephen P. Long

Citation: Perez RPA, Vezy R, Brancheriau L, Boudon F, Grand F, Ramel M, Artanto Raharjo D, Caliman J-P, Dauzat J. 2022. When architectural plasticity fails to counter the light competition imposed by planting design: an *in silico* approach using a functional–structural model of oil palm. *In Silico Plants* **2022**: diac009; doi: 10.1093/insilicoplants/diac009

ABSTRACT

Functional–structural plant modelling approaches (FSPM) explore the relationships between the 3D structure and the physiological functioning of plants in relation to environmental conditions. In this study, we present a methodological approach that integrated architectural responses to planting design in an oil palm FSPM, and test the impact of planting design and architectural plasticity on physiological responses such as light interception and carbon assimilation. LiDAR-derived and direct measurements were performed on five planting designs to assess the phenotypic plasticity of architectural traits, and allowed evaluating the variations of the main parameters of an existing 3D plant model. Accordingly, we proposed a neighbourhood index (NI) as a simple explanatory variable of architectural plasticity, and used NI-based allometries to simulate architectural variations in 3D virtual plants. Light interception and carbon assimilation were then simulated on virtual plots reproducing the five studied designs. We found that the main traits affected by plant proximity were leaf dimensions, leaf weight and leaf erectness, whereas other structural traits like the frequency of leaflets along the rachis or biomechanical properties of leaves remained unchanged. Our simulation study highlighted model compliance to reproduce architectural plasticity and illustrated how architectural plasticity improved light interception via leaf area expansion, but how the competition for light imposed by the design can counterbalance this benefit in terms of carbon assimilation at stand scale. We conclude on the importance of planting patterns for plants with low architectural plasticity such as oil palm, and how *in silico* experiments can help in designing innovative planting patterns.

KEYWORDS: *Elaeis guineensis*; FSPM; LiDAR; phenotypic plasticity; plant architecture; planting design

1. INTRODUCTION

The way plants are spatially organized in a field constitute one of the major factors of agronomic performance. For food crops, the increase in yield during the green revolution has mainly come from the increase in planting densities together with the selection of genetic material adapted to these densities (Kush 2001; Assefa *et al.* 2018). The ability to increase agronomic performance by increasing density is species-specific and depends on the capacity of plant to tolerate high density, due to the antagonistic effect between per-plant yield and density tolerance (Assefa *et al.* 2018). Oil palm (*Elaeis guineensis*) and coconuts are not an exception to the rule, the spacing between oil palm being considered as a major contributor to oil yield (Bonneau *et al.* 2014). However, experimentation on perennial crops such as oil palm requires long and expensive agronomic trials, making the testing of innovative practices rather economically risky. Investigation on optimal densities for oil palm has focused so far on the distance between plants, maintaining the conventional equilateral triangle pattern (quincunx design; Rafii *et al.* 2013; Bonneau *et al.* 2018).

Incident light is the primary resource affected by planting density, but the evaluation of the effect of density and design on light partitioning is not straightforward. Indeed, the effect of planting densities on agronomic performances is often estimated through yield, which integrates the impact of various factors such as water availability, fertilization and climate conditions. As a result, the confounding factors prevent dissecting the contribution of each factor on plant performance. Modelling approaches are relevant to address such questions since models can quantify the impact of separated processes, notably biophysical processes such as light interception.

Functional–structural plant models (FSPMs) offer the possibility to finely estimate the quantity of light intercepted by virtual 3D representations of plants (Vos *et al.* 2010). The coupling between 3D structure of plants and radiative models has multiple applications: estimating light availability for intercropping (Lamanda *et al.* 2008), assessing the influence of planting patterns in crop–weed competition for light (Evers and Bastiaans 2016), evaluating the impact of architecture manipulation on plants (Willaume *et al.* 2004; Buck-Sorlin *et al.* 2011) or designing architectural ideotypes (Sarlikioti *et al.* 2011; Da Silva *et al.* 2014). More recently, studies have used FSPM to investigate the role of phenotypic plasticity in light capture and partitioning in plant mixtures (Barillot *et al.* 2014; Zhu *et al.* 2015) and emphasized the importance of phenotypic plasticity in enhancing resource acquisition.

Phenotypic plasticity is defined as morphological, architectural and physiological responses triggered by resource limitation to cope with environmentally induced stress (Valladares *et al.* 2007; Pierik and Testerink 2014). For crops growing in open habitats, limitation in light due to competition triggers shade-avoidance syndrome (SAS), a growth response to escape shade (Aphalo *et al.* 1999; Franklin 2008; Ballaré and Pierik 2017). Architectural responses associated with SAS vary among species, but generally result in stem and leaf elongation, hyponasty and reduced branching (Gommers *et al.* 2013; Pierik and De Wit 2014). Light conditions determined by neighbouring plants, more precisely the decrease in the ratio of red (R) and far red (FR) light intensity (R:FR), have been characterized as the signal-triggering SAS (Ballaré *et al.* 1990). The consequence of SAS on plant performance can be assessed through FSPM by simulating light quality within the canopy and calibrating response curves between R:FR and trait value (Chelle *et al.* 2007). This modelling approach revealed to be efficient to accurately simulate photo-morphogenesis responses such as internode elongation on cucumber (Kahlen and Stützel 2011) or wheat tillering (Evers *et al.* 2007). However, such approach can be intense in computational time and raises some methodological questions such as where on the plant and over what period of time the R:FR signal has to be perceived to trigger plant response (Demotes-Mainard *et al.* 2016; Lecarpentier *et al.* 2019). Lecarpentier *et al.* (2019) alternatively proposed a simple proxy of R:FR based on a neighbourhood green area index (GAI) that virtually mimicked the cessation of tillering in wheat.

In the present study, we wanted to address the question of how planting design modulates oil palm individual and stand performances in term of light interception and carbon assimilation, and what is the contribution of architectural plasticity to these performances. Using comprehensive and destructive data of plant architecture and vegetative biomass measured on five planting designs, we assessed oil palm phenotypic plasticity. The integration of the observed architectural plasticity into an existing FSPM of oil palm (Perez *et al.* 2016) allowed us conducting a simulation study to test the impact of planting design and architectural plasticity on physiological processes such as light interception and carbon assimilation.

2. MATERIALS AND METHODS

2.1 Experimental site

Field measurements were performed in experimental plots at the SMART Research Institute (SMARTRI, Smart Tbk.) located near Pekanbaru (Riau Province, Sumatra, Indonesia). This study focused on five plots with different planting density, varying from 136 (conventional) to 272 plants per hectare. Besides variations in planting density, the designs also varied from the conventional quincunx design with anisotropic patterns, i.e. involving non-equivalent distances between plants. Table 1 shows the characteristics of the five designs: isotropic when plants present equivalent distance to all their neighbours and homogeneous when all plants share a unique neighbourhood pattern [**see Supporting Information—Fig. S1**]. A heterogeneous design means that replicating a single neighbourhood pattern is not sufficient to represent the entire design. As the result, the heterogeneous design C is defined by two groups of plants (p1 and p2). The trial was set up in 2013 and each plot was planted with oil palm plants (*E. guineensis*) with a genetically uniform material (one progeny) grown in nursery for 18 months after seedling germination.

2.2 Phenotyping architectural plasticity

Destructive measurements were conducted in July 2019 (i.e. ~72 months after planting) to estimate plant dimensions and biomass. Six plants per plot, selected in the middle of each plot to avoid any border effects, were entirely dissected to collect structural, geometrical and biomass data for all leaves. Structural data included the number of leaves and the number of leaflets per leaf. Rachis and petiole length, fresh and dry weight were also measured along with the length, maximal width and fresh and dry biomass of a subsample of four leaflets

Table 1. Characteristics of the five studied planting patterns. Distance min, mean and max indicate the minimal, the average and the maximal distance between plants, respectively. Design C presents two groups of plants due to the irregular spacing between plants in the plot.

Design	Density (plants per hectare)	Pattern	Distance min (m)	Distance mean (m)	Distance max (m)	Polygon area (m^2)
A	136	Isotropic homogeneous	9.21	9.21	9.21	220
B	272	Anisotropic homogeneous	4.61	7.07	8.31	110
C	272	Anisotropic heterogeneous	3.07 (p1) 8.12 (p2)	5.60 (p1) 8.49 (p2)	8.13 (p1) 9.21 (p2)	49 (p1) 171 (p2)
D	200	Anisotropic homogeneous	5.00	8.54	10.31	117
E	200	Anisotropic homogeneous	6.01	7.07	10.00	150

per leaf. For each design, measurements were performed on two replicated plots and data of the two plots were pooled together after checking that plot effect was negligible in comparison to design effect [**see Supporting Information—Table S1 and Fig. S2**]. As a result, 12 plants per design (even though being pseudoreplicates) were pooled together and considered for the analyses performed on structural data.

Dedicated measurements for estimating the biomechanical properties of the leaves were collected on December 2019 on one of the two plots. Three plants per plot were selected on which three leaves located at the top, middle and bottom of the crown were sampled. For each leaf, the length and declination, i.e. the angle from the vertical plane at leaf insertion on the stem, were measured, and remarkable points on the leaf nerve were identified (**see Supporting Information—Fig. S3**; Perez 2017). The 3D coordinates of these points along the rachis were manually reported for describing leaf bending and deviation (Perez 2017 Appendix A for the methodology). Each leaf was then cut into four segments between each remarkable point, and provided the following information at each section/segment: cross-sectional shape (width and thickness), length and fresh weight of the rachis segment, fresh weight of the leaflets on segment. These geometrical and biomass attributes were subsequently used to calibrate the biomechanical modulus of the leaves (cf. next section).

Field measurements of leaf architecture, mainly leaf angles and 3D coordinates, were hardly feasible on a high number of plants and may be very sensitive to manipulators. Here we tested how LiDAR-based measurements could overcome those phenotyping constraints. Terrestrial LiDAR (TLS) scans were thus collected on five palm trees to derive phenotypic traits of leaf geometry that were compared to labour-intensive measurements. Reflective balls and stripes were placed on rachis base (point C) and tip (point A) to easily identify these points on the TLS scans. On average, four scan positions were needed around each plant to isolate and clean co-registered 3D points of leaves. The PlantScan3D software (Boudon *et al.* 2014) was used to manually retrieve the 3D coordinates on the collected point clouds along the rachis and determined rachis length, bending and deviation (Fig. 1). Comparison of TLS-derived data and handmade direct measurement were assessed through root mean square error (RMSE), normalized root mean square error (NRMSE) and bias defined as:

$$RMSE = \sqrt{\frac{\sum_{i=1}^{n}(t_i - m_i)^2}{n}}$$

$$NRMSE = \frac{\sqrt{\frac{\sum_{i=1}^{n}(t_i - m_i)^2}{n}}}{\sum_{i=1}^{n} m_i / n}$$

$$bias = \frac{\sum_{i=1}^{n}(t_i - m_i)}{n}$$

where t_i and m_i are TLS observations and handmade observations, respectively, and n represents the number of observations.

2.3 Leaf biomechanical model

The biomechanical model of leaf aimed at simulating leaf deformation (due to bending and torsion) according to leaf geometry, biomass and its biomechanical properties. Leaf geometry inputs (rachis length and cross-section width and thickness) were modelled using the existing VPalm allometries (Perez *et al.* 2016, 2018) and updated to take into account the architectural plasticity with planting density. New allometries were defined to link leaf length and leaf biomass, and allowed the estimation of rachis biomass properties required in the biomechanical model.

Due to the slenderness of the rachis (ratio length to cross-section dimensions), the biomechanical model considered the rachis as a beam subjected to two combined stresses: a bending stress and a torsion stress. The transverse shear deformation in the cross-section was neglected (slender beam). The constitutive equations of the beam theory (Euler–Bernoulli beam theory) in mechanics of solids can be applied in their integral forms, which allow varying the modulus of elasticity within the cross-section and along the length, as the inertia along the length of the beam. Furthermore, considering the integral forms, the initial shape of the beam can be curved. Theses equations are valid only for small displacements, but can be used to obtain large displacements via a decomposition of the total loading in successive elementary loadings.

To simplify the model (and to allow a determination of the modulus of elasticity), the shear modulus (G) and the modulus of elasticity (E) were considered constant along the rachis and were used to model the torsion and the bending of the rachis, respectively. Besides, we assumed that biomechanical properties were independent of leaf age. The material was assumed to be homogeneous and isotropic in the cross-section. Bending and torsion inertia were estimated for each of the five remarkable points using simple geometrical cross-sectional shapes (C: down triangle, CB: rectangle, B: up triangle, BA: ellipse, A: circle).

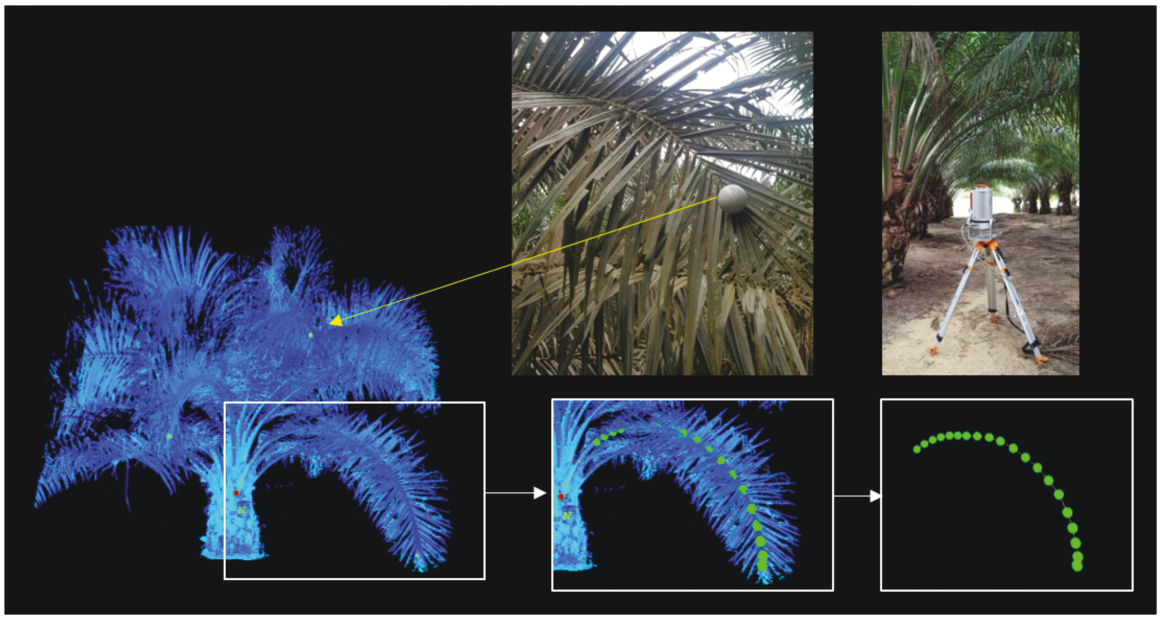

Figure 1. Processing terrestrial LiDAR scans on PlantScan3D software to retrieve 3D coordinates along the rachis.

The rachis was discretized in 100 segments to solve numerically the integral forms of the constitutive equations (the cross-sections were discretized in 100 × 100 pixels and the inertia values were interpolated between the five remarkable points). The total loading (due to the segment weights and leaflet weights) was decomposed in a sum of 'elementary loadings', so that each elementary loading induced small displacements (the assumption of small displacement is checked at each computation step all along the beam). A computation step corresponded to the application of an elementary loading on the previous deformed shape of the beam (deformed shape obtained at the previous step). This iterative method on the loading allowed obtaining large displacements of the rachis. The final deformation was thus the result of a successive number of combined bending and torsional elementary deformations resulting from the segment mass and inertia.

The shear modulus (G) was experimentally estimated with a dedicated device [**see Supporting Information—Appendix S1; Fig. S4**] and an average value was calculated for each density. The modulus of elasticity (E) was estimated from an optimization process on the 3D coordinates derived from field measurements. The optimization processes to estimate the value of E for each leaf used the value of G obtained experimentally, and the measurements of rachis segment biomass, length and cross-sectional shapes. Using the Nelder–Mead simplex algorithm (Nelder and Mead 1965; Lagarias *et al.* 1998), the optimization consisted in finding the value of E that minimized the quadratic error (EQ) between simulated coordinates and the experiment [**see Supporting Information—Fig. S5**].

$$EQ = \sqrt{\frac{\sum_{k=1}^{N_{pts}} (X_{Exp} - X_{Sim})^2}{N_{pts}}} + \sqrt{\frac{\sum_{k=1}^{N_{pts}} (Y_{Exp} - Y_{Sim})^2}{N_{pts}}} + \sqrt{\frac{\sum_{k=1}^{N_{pts}} (Z_{Exp} - Z_{Sim})^2}{N_{pts}}}$$

where:

N_{pts}: the number of experimental points (five points)
X, Y, Z_{Exp}: the observed coordinates in field
X, Y, Z_{Sim}: the simulated coordinate for given E and G values

The initial solution to start the simplex was set to a value of 1000 MPa (this value was chosen after static tests performed on some rachis samples to determine the modulus of elasticity).The optimization was performed on each of the 15 leaves studied per density and the average value of E was calculated for each density.

2.4 Defining a neighbourhood index to model architectural plasticity

Changes in architectural attributes in response to planting design were considered at a given developmental stage (6 years after planting). The integration of plasticity in the VPalm 3D model required the development of allometries based on a variable as generic as possible able to decipher each of the designs considered in our study. In this study, some designs presented similar density with varying pattern (Table 1). As a result, planting density was not alone informative enough to decipher the designs.

Various neighbourhood indices, derived from distances between plants, were tested to establish the existence of simple allometries with VPalm parameters. The indices tested were the minimal, average and maximal distance between plants and the polygonal area around the central plant defined by the closest surrounding plants (**see Supporting Information—Fig. S1**; Table 1). As for planting density, the average and the maximal distances between plants did not allow to properly decipher the studied designs. Contrarily, the minimal distance between plants proved to be unique for each pattern and was thus considered as the explanatory variable of plastic

responses. Polygonal area and the minimal distance between plants were highly correlated [**see Supporting Information—Fig. S6**], therefore involving comparable allometries. We investigated the existence of simple relationships between the minimal distance (hereafter called neighbourhood index [NI]) and the variations of VPalm parameters with designs. VPalm allometries (Perez *et al.* 2016) were fitted on the observed data for each plant (Fig. 2A and B) and regression analyses were performed to evaluate if NI was a significant factor in the adjustment of allometric parameters. When significant differences were found, i.e. when the coefficient associated to NI was significantly different from zero (*P*-value of the *t*-test < 0.05; Table 2), NI was selected as the explanatory variable for rendering architectural plasticity and NI-based allometries were defined to simulate VPalm parameter values (Fig. 2C and D). Architectural plasticity was estimated for each parameter as the relative variation of the parameter from its value on the reference design (NI = 9.21 m).

2.5 Evaluating the effect of planting design and architectural plasticity on light interception and carbon assimilation

Three-dimensional mock-ups were generated from a set of VPalm parameters derived from the NI-based allometries. Replicates of the same mock-up were placed in virtual scenes with periodic boundary conditions to reproduce the planting designs with endless canopies (Perez *et al.* 2018). Inter-individual variability was generated thanks to the dedicated variance parameters in VPalm rendering variations in the allometric relationships (Perez *et al.* 2016). Subsequently, for each design, variations in leaves geometrical attributes (length, declination and number of leaflets) and leaflets dimensions (length and width)

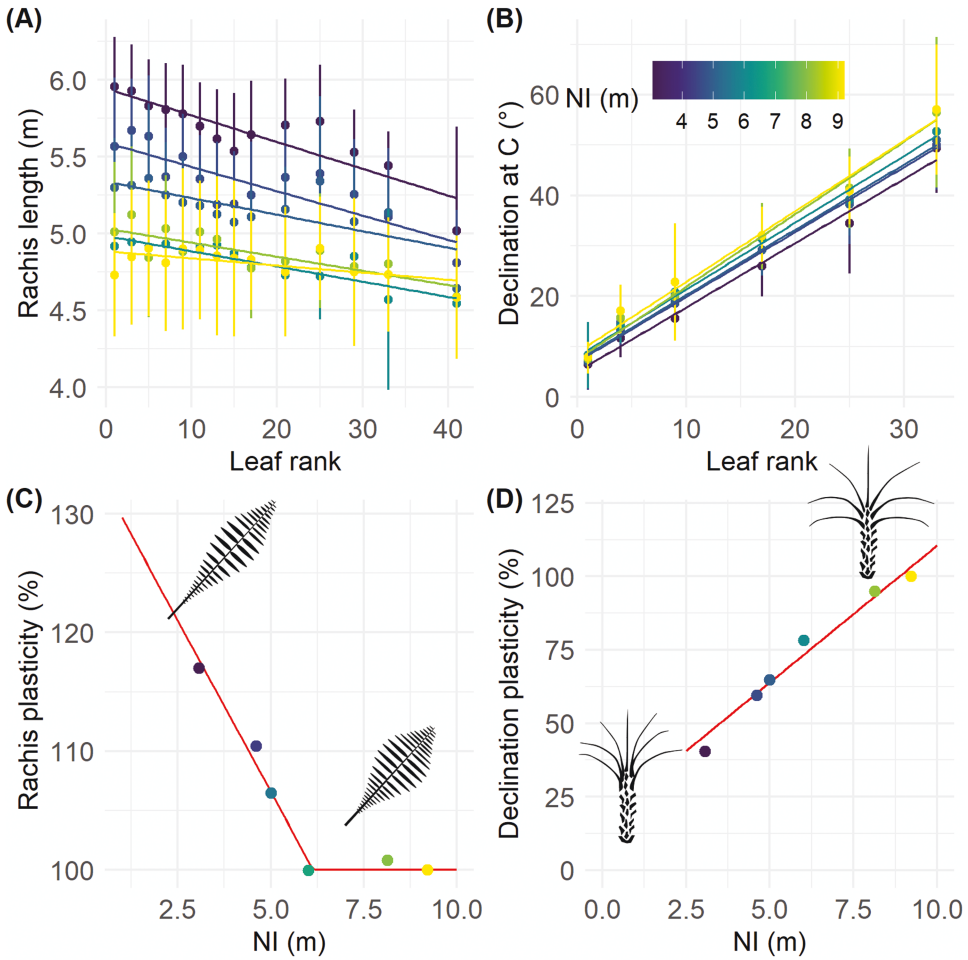

Figure 2. Allometries derived from neighbourhood index to model architectural plasticity. Observations and VPalm allometries fitting for rachis length (A) and rachis base declination (B) used for estimating the variation in model parameters with NI (points indicate average value per rank and design, vertical lines standard deviations between individuals). Allometries were fitted for each design with one of the two parameters constant (here the slope), the other parameter being used to define the NI-based allometric relationships (C and D). Rachis length plasticity (C) and declination plasticity (D) represent the percent of variation of rachis length intercept and the declination intercept (relatively to the control design NI = 9.21 m), respectively.

Table 2. Calibration of VPalm parameters in response to NI. When significant relationships between a parameter and NI are stressed, the allometric equation is written in the parameter value. Level of significances correspond to the *P*-value of *t*-test (ns, non-significant; ***P* < 0.01; ****P* < 0.001).

Predicted variable	VPalm equation	Parameter	Significance level with NI	Parameter value
Rachis length	$L_{rac} = L_{rac\ int} + L_{rac\ slp} \times rank$	$L_{\text{rac int}}$	***	$L_{rac\ int} = \begin{cases} 505 \times (1.35 - 0.058\ NI), & NI < 6.14 \\ 505, & NI \geq 6.14 \end{cases}$
		$L_{\text{rac slp}}$	ns	$L_{\text{rac slp}} = -1.45$
Petiole length	$L_{pet} = L_{rac} \times ratio_L$	ratio_L	ns	$\text{ratio}_L = 0.25$
Relative position of point B on rachis		PosB_{rel}	ns	$\text{PosB}_{\text{rel}} = 0.66$
Number of leaflets per leaf	$Nb_{Lft} = \frac{Nb_{max}}{1+e^{4Nb_{slp}}(Nb_{infl}-L_{rac})}$	Nb_{max}	ns	$\text{Nb}_{\text{max}} = 172$
		Nb_{slp}	ns	$\text{Nb}_{\text{slp}} = 0.0025$
		Nb_{infl}	ns	$\text{Nb}_{\text{infl}} = 241$
Leaflet length	$L_{Lft\ B} = L_{B\ int} + L_{B\ slp} \times L_{rac}$	$L_{B\ \text{int}}$	ns	$L_{B\ \text{int}} = 77.7$
		$L_{B\ \text{slp}}$	ns	$L_{B\ \text{slp}} = 0.016$
Leaflet width	$W_{Lft\ B} = W_{B\ int} + W_{B\ slp} \times L_{rac}$	$W_{B\ \text{int}}$	ns	$W_{B\ \text{int}} = 4.06$
		$W_{B\ \text{slp}}$	ns	$W_{B\ \text{slp}} = 0.00097$
Declination at C point		$\delta_{C\ \text{int}}$	**	$\delta_{C\ int} = 10.1 \times (0.17 + 0.09NI)$
		$\delta_{C\ \text{slp}}$	ns	$\delta_{C\ \text{slp}} = 1.33$
Shear modulus		G	ns	$G = 125$
Elastic modulus		E	ns	$E = 3026$
Rachis fresh weight	$FW_{rac} = FW_{rac\ \text{int}} + FW_{rac\ slp} \times L_{rac}$	$FW_{rac\ \text{int}}$	***	$FW_{rac\ int} = \begin{cases} 354 \times (1.31 - 0.054\ NI), & NI < 5.75 \\ 354, & NI \geq 5.75 \end{cases}$
		$FW_{rac\ slp}$	ns	$FW_{rac\ slp} = 0.00571$

were simulated to obtain seven individual mock-ups, each randomly deriving from an average individual. Seven plots were simulated per design to reproduce inter-individual variability and its impact on physiological processes. The number of simulations (seven) was chosen to allow the estimation of the mean and standard deviation of physiological outputs, with the concern of limiting the computational time to one night. The low coefficient of variation on simulation outputs [**see Supporting Information—Table S2**] also supported the choice to conduct only few simulation repeats. Simulation of physiological processes were computed in Archimed-φ (https://archimed-platform.github.io/) using meteorological and light conditions (sun position and day length) with a 30-min time step on a sunny day in the experimental site (Pekanbaru, Sumatra). Light interception of each object (leaflet, rachis, petiole, snags and soil) was estimated on the 3D explicit stands considering 16 hemispherical directions. Direct incident light was computed for each triangle in the scene and scattered light assuming that each leaf intercepts scattered radiation proportionally to its apparent surface area in the direction of the incoming radiative flux (Dauzat *et al.* 2001).

Carbon assimilation was simulated using the model of Farquhar *et al.* (1980) coupled to the stomatal conductance model from Medlyn *et al.* (2011), and the leaf temperature by closing the energy balance (Monteith and Unsworth 2008). The long-wave radiation exchanges between the leaves and the environment were computed using a sky view angle, considering the system as isotropic except for the sky considered at air temperature (Dauzat *et al.* 2001) with constant parameters estimated on oil palm (Table 3). The model was run at a 30-min time step considering changing climate conditions over the day. The last variable was water-use efficiency (WUE), defined as the ratio between carbon assimilation and water transpiration. See Perez *et al.* (2022) for an example of the input files used for simulating design A.

The total light interception, carbon assimilation and mutual shading were compared for each design at plant and plot scale. Mutual shading was evaluated as the difference between the amounts of light intercepted by a single plant in a stand and the amounts intercepted by the same plant in isolated conditions, under similar incident radiation (Perez *et al.* 2018).

Table 3. Parameter values of Farquhar model and Medlyn model used for oil palm.

Model	Parameter	Value
Farquhar	J_{max}	250 $\mu mol_{electron} \cdot m^{-2} \cdot s^{-1}$
	V_{cmax}	200 $\mu mol_{CO2} \cdot m^{-2} \cdot s^{-1}$
	R_d	0.6 $\mu mol_{CO2} \cdot m^{-2} \cdot s^{-1}$
	Θ	0.853
	TempC ref	25 °C
Medlyn	g_0	−0.03 $mol_{CO2} \cdot m^{-2} \cdot s^{-1}$
	g_1	12

The effect of architectural plasticity on physiological processes was estimated for each design by comparing the simulation outputs obtained from the mock-up integrating changes in architecture with the simulation outputs obtained without considering these changes, i.e. using a mock-up from the control design (Fig. 3).

3. RESULTS

3.1 LiDAR-based measurements are promising for fast and accurate phenotyping of oil palm architecture

The TLS scans were processed to extract leaf 3D coordinates and derived rachis length (Fig. 1). Rachis length estimated from LiDAR data showed high accuracy in comparison with the length recorded manually, with an average error around 5 cm (NRMSE = 1 %; Fig. 4A). Terrestrial LiDAR data were also used to compare the quality of manual measurements relative to the 3D coordinates along rachis required for estimating the biomechanical modulus of elasticity (E). On average results highlighted a close match between the coordinates recorded manually and the one extracted from TLS data, but some discrepancies were revealed for some leaves [**see Supporting Information—Fig. S7**]. These differences could be explained by the impact of wind during measurements, but most probably because of leaf manipulation during manual measurements that could deform the leaves. To better estimate the effect of these differences on model calibration, both set of coordinates were used to optimize the value of elastic modulus (E), input data related to biomass remaining unchanged. Results emphasized the consistency of E between the two methodologies with an NRMSE of 8 % (Fig. 4B), and clearly showed that manual measurements have an acceptable accuracy compared to TLS.

3.2 Plant proximity increased rachis length and erectness while structural components remained unchanged

Change in architectural traits with NI was mainly observed on the rachis (rachis length, rachis fresh weight and declination at point C) while the other architectural traits remained unchanged in comparison with the conventional planting density (design A). Rachis length significantly decreased with increasing NI until a plasticity threshold estimated at NI = 6.14 m (Fig. 2C; Table 2). At the minimal NI (3.07 m; design C-p1), rachis length increased by 18 % comparatively to the reference design. With increasing plant proximity, rachis were also lighter than rachis at the conventional density (up to 27 % of decrease in rachis fresh weight), suggesting that the increase in rachis growth was at the expense of rachis fresh weight. Response to plant proximity was also revealed by an increase in plant erectness (up to 20 % reduction in declination at point C for the top crown leaves), which could be explained by lower rachis fresh weight for comparable biomechanical properties. Indeed, no significant change in elastic and shear modulus was observed among designs, revealing that change in architecture was driven by change in biomass allocation rather than in biomechanical properties.

The number of leaflets per leaf increased with increasing rachis length, but no significant effect of NI was found, suggesting that relationships between leaf dimension and leaf structural characteristics

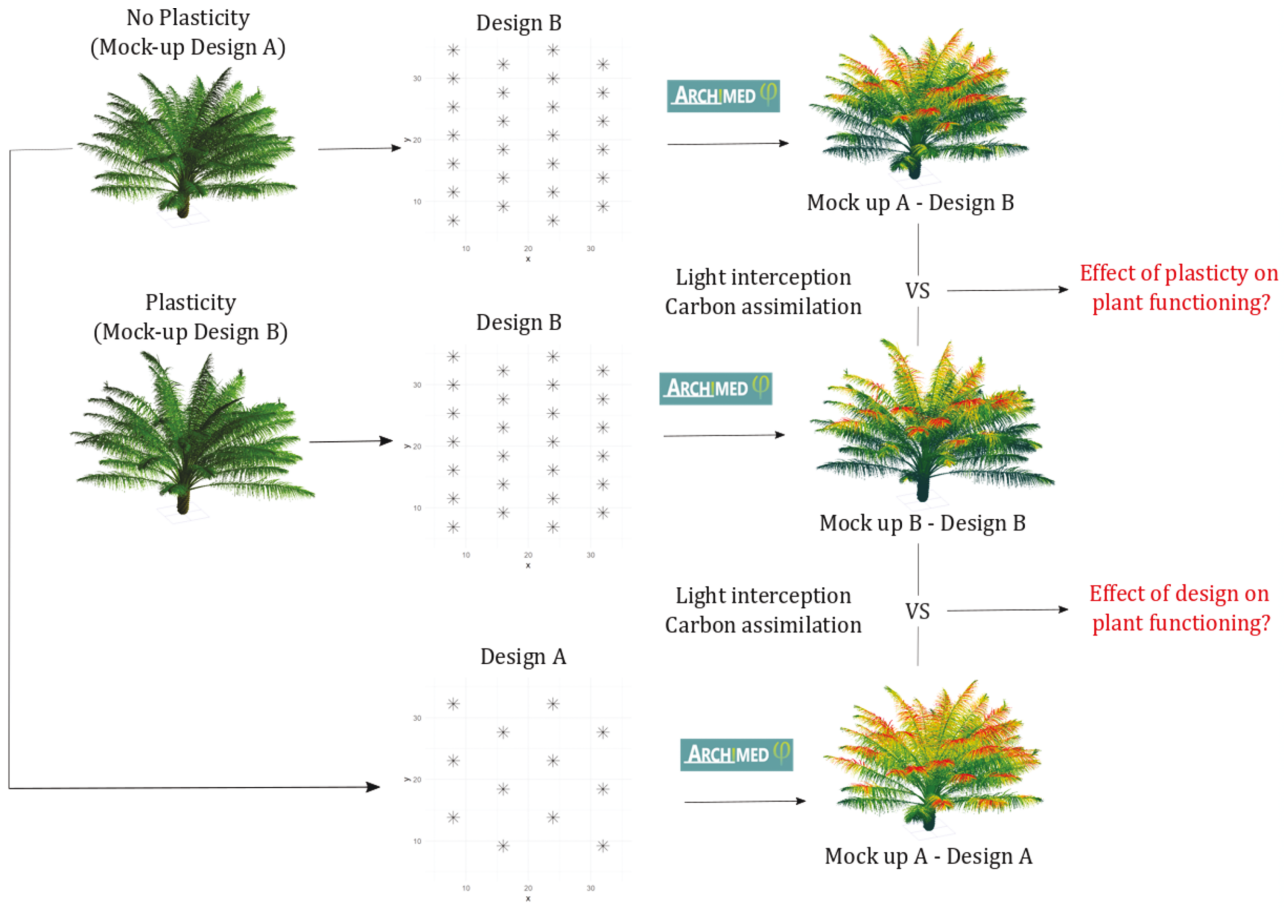

Figure 3. Simulation strategy to estimate the impact of architectural plasticity and planting design on physiological processes. Mock-up of the reference design (design A) corresponds to the model without plasticity, and is thus taken as point of comparison for estimating the impact of plasticity on physiological processes. Colours on 3D mock-up on left represent light irradiance at noon.

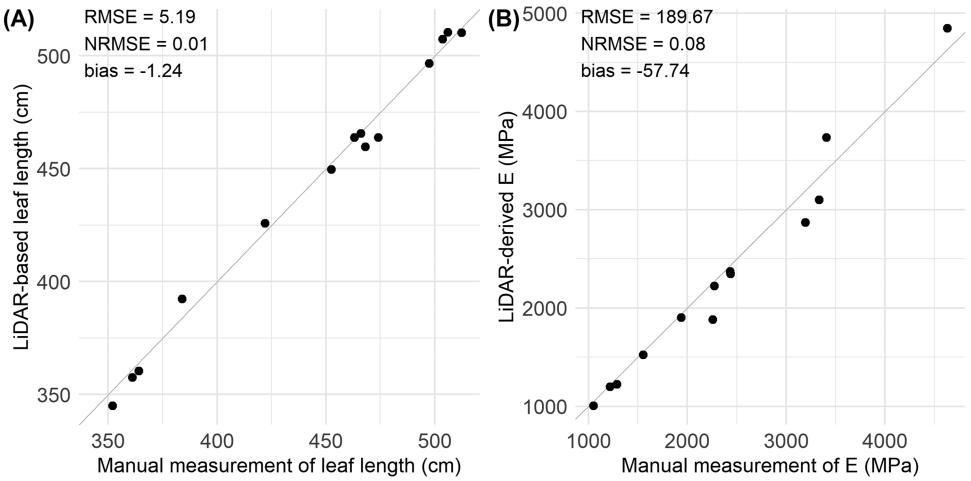

Figure 4. Comparison of manual and LiDAR-based measurement of rachis length (A) and elastic modulus *E* (B). Values of *E* are estimated using the optimization processed from 3D coordinates recorded manually or extract from LiDAR point clouds ($n = 14$ observations). Grey line represents the 1:1 line.

remained unchanged. Regarding leaflets dimensions, allometries depending on rachis length were also conserved highlighting negligible effect of NI on leaf structure.

3.3 NI-based allometries correctly render architectural plasticity among planting designs

Statistical analyses allowed the evaluation of the architectural parameters significantly affected by NI, and NI-based allometries were derived to predicted parameter values depending on design (Table 2). No significant effect of NI was found on leaflet attributes (number, length and width). Given that leaflets were modelled thanks to allometries based on rachis length, it was likely that the effect of NI on leaflets was already integrated through the differences in rachis length. In other words, the relation between rachis length and leaflets attributes was not modified depending on design. The potential errors resulting from the successive assembly of NI-based allometric relationships with VPalm allometries were then assessed through the comparison of trait values simulated and measured in field. Simulations were performed using the average parameters estimated for each design, setting to zero all the variances parameters used to generate inter-individual variability in VPalm (Perez *et al.* 2016). Results highlighted model compliance to reproduce architectural plasticity through NI-based allometric relationships (Fig. 5). The model allowed the simulation of the increase in rachis length and the decrease in rachis fresh weight with plant proximity (Fig. 5A and B). The comparison of the VPalm model with and without NI-based allometries showed the benefits of the integration of plasticity on the model. For instance, prediction errors (NRMSE) for rachis length decreased from 10 to 3 %, from 21 to 9 % for rachis fresh weight and from 16 to 6 % for declination at C point. For the other traits that did not show significant change with NI, for instance the number of leaflets per leaf, simulations revealed less compliance to observations (Fig. 5D). Results on leaflets dimensions (Fig. 5E and F) exhibited higher variations in observations than in simulation, revealing the limits of the model to simulate the observed variations at the leaflet scale. It is however worth noting that observed coefficient of variation in leaflets dimensions was very low (below 5 %), which could explain the incapacity of the model to render such precision in predictions.

3.4 Improvement of resources acquisition through architectural plasticity is outdone by planting design

The estimation of total plant leaf area is not straightforward for oil palm since it integrates the area of thousands of leaflets. VPalm

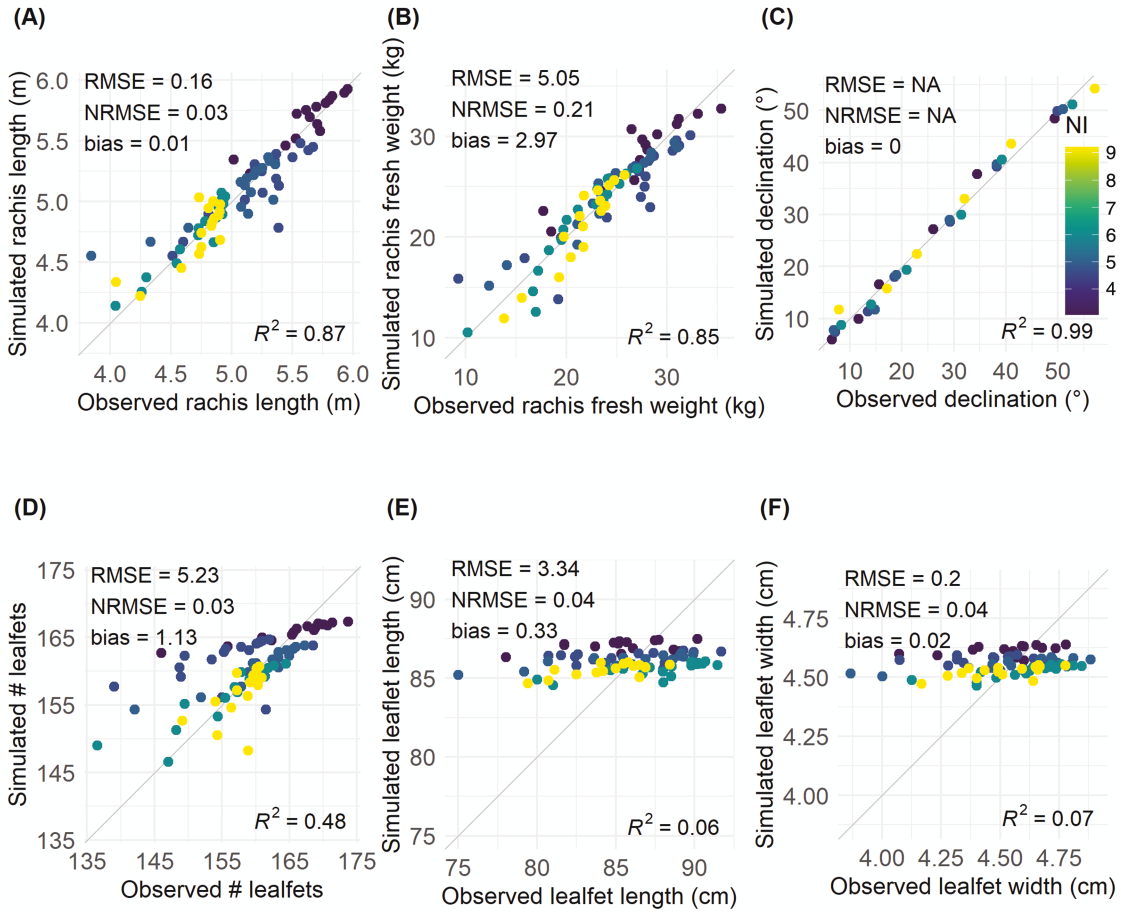

Figure 5. Comparison of trait values observed in field and simulated in the VPalm model taking into account influence of the NI factor. Points indicate average value per leaf rank for each design (colours = NI value). Grey line represents the 1:1 line.

simulations allowed the estimation of total plant leaf area and can be used to compare leaf area between designs. Increase in rachis size resulted in a global expansion in plant leaf area, but was only stressed for the design B, C-p1 and D, with a gain varying from 4 to 10 % in comparison to the conventional design A (Fig. 6). Combined to the radiative balance model, 3D mock-ups enabled comparison of the impact of architecture and design on light interception and the related biophysical processes [**see Supporting Information—Fig. S8**]. The design A proved to be the most efficient to maximize resources acquisition at the plant scale: the amount of light intercepted, carbon assimilated and water transpired being markedly higher for this design than the four other designs. For instance, in high density rows of design C (p1), plants presented 43 % less intercepted light and 54 % less carbon acquisition in comparison with design A. Only the design D presented an equivalent level of transpiration, and reduction in light capture, carbon assimilation and WUE below 5 %. The better resource acquisition in design A was mainly explained by the lower mutual shading conferred by its lower planting density compare to the four other design but also because the quincunx design which allowed a homogeneous repartition and a better penetration of light within the crown (Fig. 7). The design D also highlighted a good penetration of light, with a global mutual shading of 23 %. Design A presented the best penetration of light within the canopy due to the lower total leaf area, but it is worthy to note that, at the leaf area index (LAI) of design A (around 2.7 $m^2 \cdot m^{-2}$), design D presented inferior value of mutual shading than design A. As a result, it is likely that competition for light in design D became lower that design A when plants reach maturity.

Outputs at the stand scale highlighted the importance of planting design on physiological processes (Fig. 8). Interestingly, we found a trade-off between resource loss at the plant scale (Fig. 6) and performance gain at stand scale due to higher planting density. Increased density globally improved light interception (from 9 to 44 %), but gain in carbon assimilation was not correlated to the gain in light interception. For instance, the gain in light interception due to the high density in design E did not counterbalance the negative impact on photosynthesis at the plant scale. Indeed, the total carbon assimilated per hectare in design E remained close to design A. Only designs B and D highlighted the benefits of higher density on carbon gain at the stand scale, with 13 % and 42 % more carbon assimilated than the conventional design, respectively. Regarding WUE (Fig. 8D), design A demonstrated the highest value but design D confirmed to be an interesting design with only 3 % lower WUE compared to the design A.

When comparing simulations with and without architectural plasticity, the increase in total leaf area only demonstrated little gain in light capture and carbon assimilation (Fig. 8A and B). Even if the plasticity effect resulted in more erected leaves, the spatial arrangement of leaves did not prevent extra leaf area to increase mutual shading, except for design E (Fig. 8C). Gain in carbon assimilation due to plasticity was eventually negligible, with a maximum of 2 % for design C and D. As a result, the potential gain at the plant scale in light capture and carbon assimilation due to plastic response (leaf area expansion and leaf erectness) under higher density did not overcome the biophysical drawbacks of competition for light.

4. DISCUSSION

4.1 Phenotyping oil palm architecture with LiDAR

Phenotyping plants in the field usually requires techniques that are laborious, time-consuming and destructive. This is particularly true for 3D data, which can be very sensitive to manipulators or equipment, involving bias with consequences hardly predicable. LiDAR-based phenotyping is a promising technology to overcome these drawbacks (Lin 2015; Furbank *et al.* 2019). Here we found close match between LiDAR and manual measurements, for both dimensions and 3D coordinates of oil palm leaves, suggesting that both methods can be used for accurately phenotyping these traits. The added value of LiDAR measurements remains in the possibility to screen 3D architecture without manipulating leaves, contrarily to handmade measurements that often requires deforming or even cutting the leaves. In addition, LiDAR offers the capacity to phenotype tall palms, which are difficult to access manually, and makes architectural measurements on old stands possible. Scanning plants with TLS can simultaneously and rapidly collect data on several organ or plants, but often requires multiple views to avoid occlusion problem (Thapa *et al.* 2018). When field conditions are windy, the subsequent co-registration of scans introduces noise in the point clouds, decreasing data quality for post-processing. Nowadays, post-processing is the main bottleneck in LiDAR-based measurement, since manual work on point clouds is still needed to extract trait value. As a result, the time saved in collecting scan in field, in comparison to traditional measurements, can be lose afterwards in computational processes. In the present study, post-processing was supported by the software PlantScan3D (Boudon *et al.* 2014), which provided a semi-automatic methodology to rapidly extract 3D coordinates along rachis nerve. Enhancement of the current method could be achieved to render the process fully automatic, for instance using deep learning method allowing automated segmentation of leaves and extraction of phenotypic properties (Ziamtsov and Navlakha 2019). It is worth to precise that such improvements could be achieved rapidly on few traits like rachis length, shape and angles. Nevertheless, regarding other traits like biomass components or leaflets counts for instance, further technical improvements and dedicated data set would be required.

4.2 Towards a model of oil palm that accounts for architectural plasticity over plant development

The present study indicated the main changes in oil palm architecture in response to plant proximity. The increase in rachis length confirmed the results obtained by Bonneau *et al.* (2014), which showed significant frond length difference among planting density starting from 72 months after planting (same stage than the present study). Bonneau *et al.* (2014) observed significant increase in frond length for densities below a distance of 8 m between plants, whereas in our study we found plastic response below 6.14 m (Table 2). The plant proximity threshold was not fully in accordance between the two studies, which could be explained by the asymmetrical designs changing incoming light at equivalent density. The increase in rachis length in response to increasing competition for light confirmed the role of leaf expansion to capture more light, as demonstrated in the sensitivity analysis previously performed on VPalm (Perez *et al.* 2018).

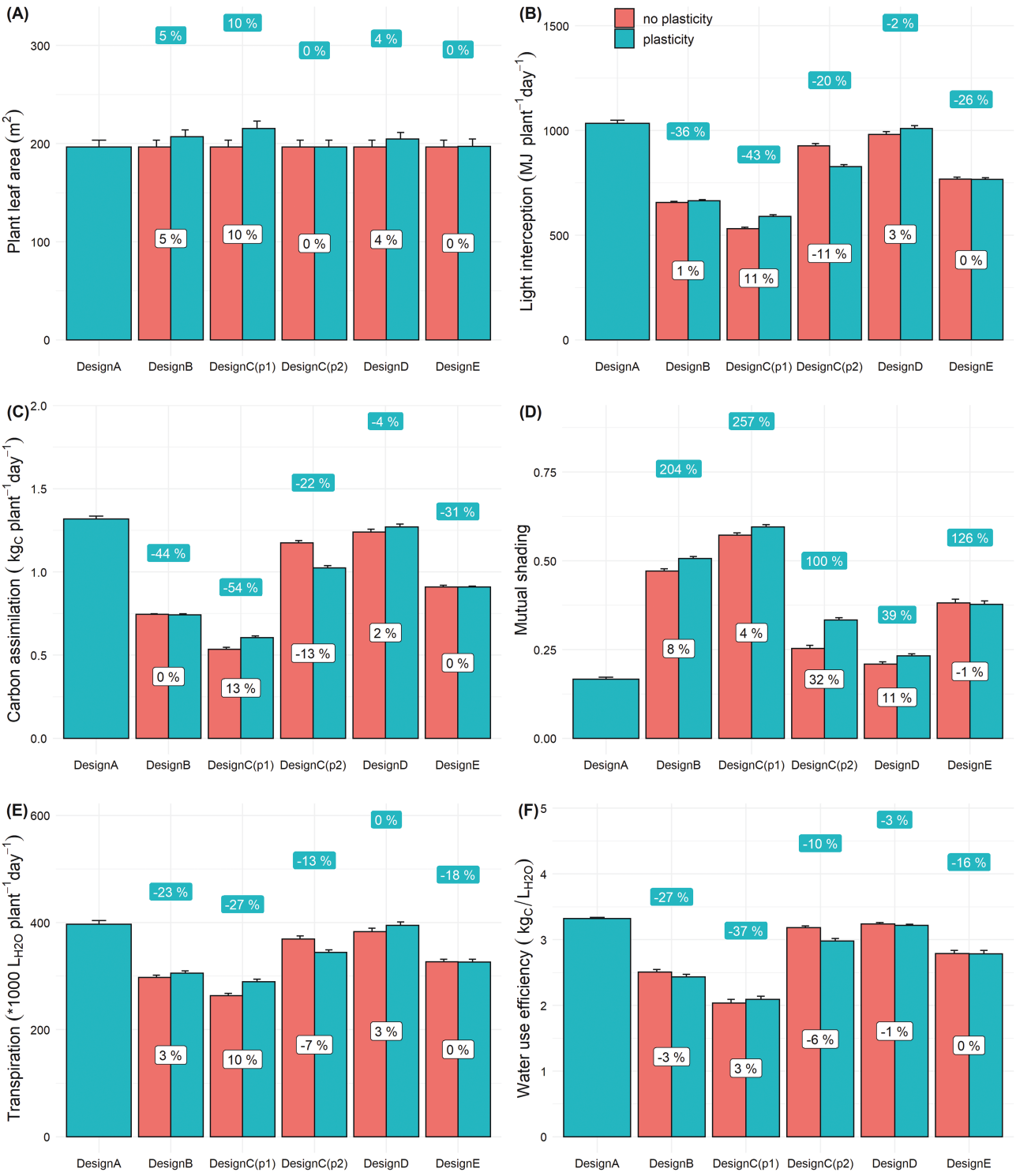

Figure 6. Simulation outputs at the plant scale for each design using plastic responses in the model (blue boxes) or not (red boxes). Bars indicate mean values and error bars standard deviation of the seven virtual individuals. Values in blue labels on top of bars represent inter-design comparison, i.e. gain or loss relatively to the design control (design A). Values in white labels on bars represent the gain or loss when architectural plasticity is considered in simulations. Design C presents two groups of plants due to the irregular spacing between plants in the plot.

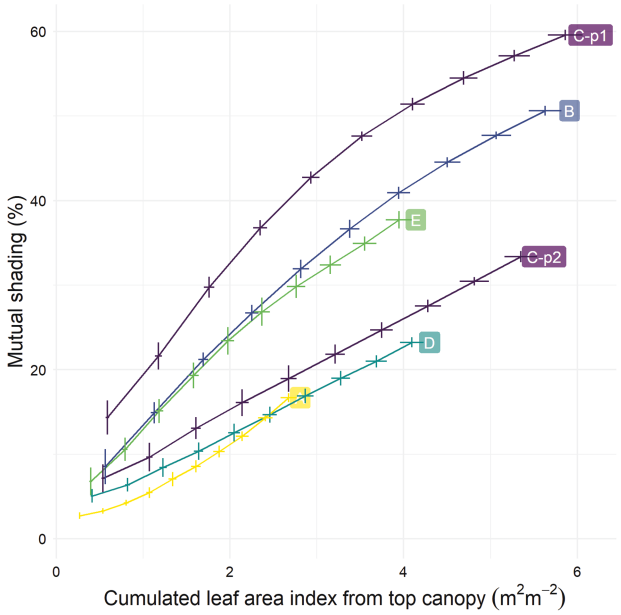

Figure 7. Mutual shading with cumulated leaf area index with canopy deepness for the five studied designs (indicated by colours and labels). Mutual shading is calculated from the difference in light intercepted within the canopy of an isolated plant and the same plant in stand. Points represent average mutual shading depending on canopy deepness; vertical lines the standard deviation between individuals. Design C presents the two groups of plants due to the irregular spacing between plants in the plot.

In many crops, plants with more erected habit are less competitive for light and thus can be planted at higher density (Reynolds *et al.* 2000; Truong *et al.* 2015; Perez *et al.* 2019). Here we observed that to avoid competition for light, oil palm modulate leaf erectness and confirmed the SAS observed on other crops (Gommers *et al.* 2013). To our knowledge, this work is a first attempt to evaluate the plasticity of biomechanical properties of leaves. We found that oil palm erectness was likely modulated through a decrease in rachis fresh weight rather than a significant change in biomechanical properties of leaves. However, further dedicated studies are needed since the ratio between rachis length and biomass was not constant depending on design, pointing out the potential existence of differences in water content and/or structural composition. Moreover, the biomechanical model presented in this study considered a unique value of elasticity and shear modulus along the leaf and with leaf age, but it is likely that properties change with space and time.

NI-based allometries allowed to correctly render the architectural plasticity observed in field, and enabled generating 3D mock-ups reproducing the main geometrical changes in response to planting design. The major limitation of the proposed approach is that the allometries are specific to the developmental stage of oil palm (72 months after planting), and therefore requires additional experiments and analysis to be generalize for younger or older stages. Indeed, it is clear that competition for light will depend on plant age: no competition in the early stages to high competition in the mature stage. One limitation of using only the nearest distance as an explanatory variable for architectural plasticity is that it does not account for other distances in anisotropic patterns (e.g. inter-row distances). The limited subset of planting patterns studied prevented us for measuring the effect of inter-row distances beyond a certain threshold, and thus from inferring architectural plasticity to broader designs. The NI proposed is biased because it only accounts for distance between plants, without considering crowns proximity (distance between leaf tips) which affects light change over time and plant development. A way to account for the dynamic changes in competition for light in relation with plasticity would be to simulate a signal which evolves with plant growth and that can trigger plastic responses beyond a given threshold. This could be achieved by directly simulating R:FR ratio (Evers *et al.* 2007; Kahlen and Stützel 2011; Bongers *et al.* 2018) in virtual scenes, but would raise questions about how to integrate the signal in time and space while adopting a parsimonious model and with reasonable computational time. As proposed by Lecarpentier *et al.* (2019), GAI can be used as a simple environmental cue of light competition. Another option could be to use directly the mutual shading as the triggering signal. It is likely to be the variable that represents the best the competition for light, but the computational cost to estimate it is still a bottleneck. One could suggest to perform simulations with a simpler approach using voxel-based (Munier-Jolain *et al.* 2013) or envelope-based (Duursma *et al.* 2012; Louarn *et al.* 2012) models, enabling fast calculation of light interception and mutual shading. In any case, the development of a dynamic approach of architectural plasticity would need phenotypic data over a period from early to mature stages. The data available for this study only concerned a relatively short period compared to oil palm development. Besides, the development of the palms has most certainly not reached a stable level, which is often observed at a later age of the plants. The ongoing collection of data in this trial would enable the development of a more integrated and generic modelling approach.

4.3 A limited architectural plasticity compensated by plasticity in carbon allocation

Our study allowed estimating the contribution of architectural plasticity in light interception, carbon allocation and WUE. Interestingly, we demonstrated that the expansion in leaf area in response to shade enabled to enhance light harvesting and increased assimilate supply at the plant scale, but also decreased WUE. Our results emphasized the trade-off between plant performance and stand performance, since higher plant density did not increase carbon assimilation at the plot scale (Fig. 8B). In this agronomic context, the similar and simultaneous plastic behaviour of plants has generated an environmental neighbourhood highly competitive for light. The monocaulous habit of oil palm architecture did not allow limiting mutual shading while expanding leaf, rendering the competition for light ineluctable. We conclude from this simulation study that, under the light stress imposed by planting design, oil palm presented a maladaptive plasticity (futile elongation of leaves) which negatively impacted community performance (Valladares *et al.* 2007). One can suggest that the limited architectural plasticity of oil palm can be compensated by the high plasticity of oil palm in term of biomass allocation (Legros *et al.* 2009).

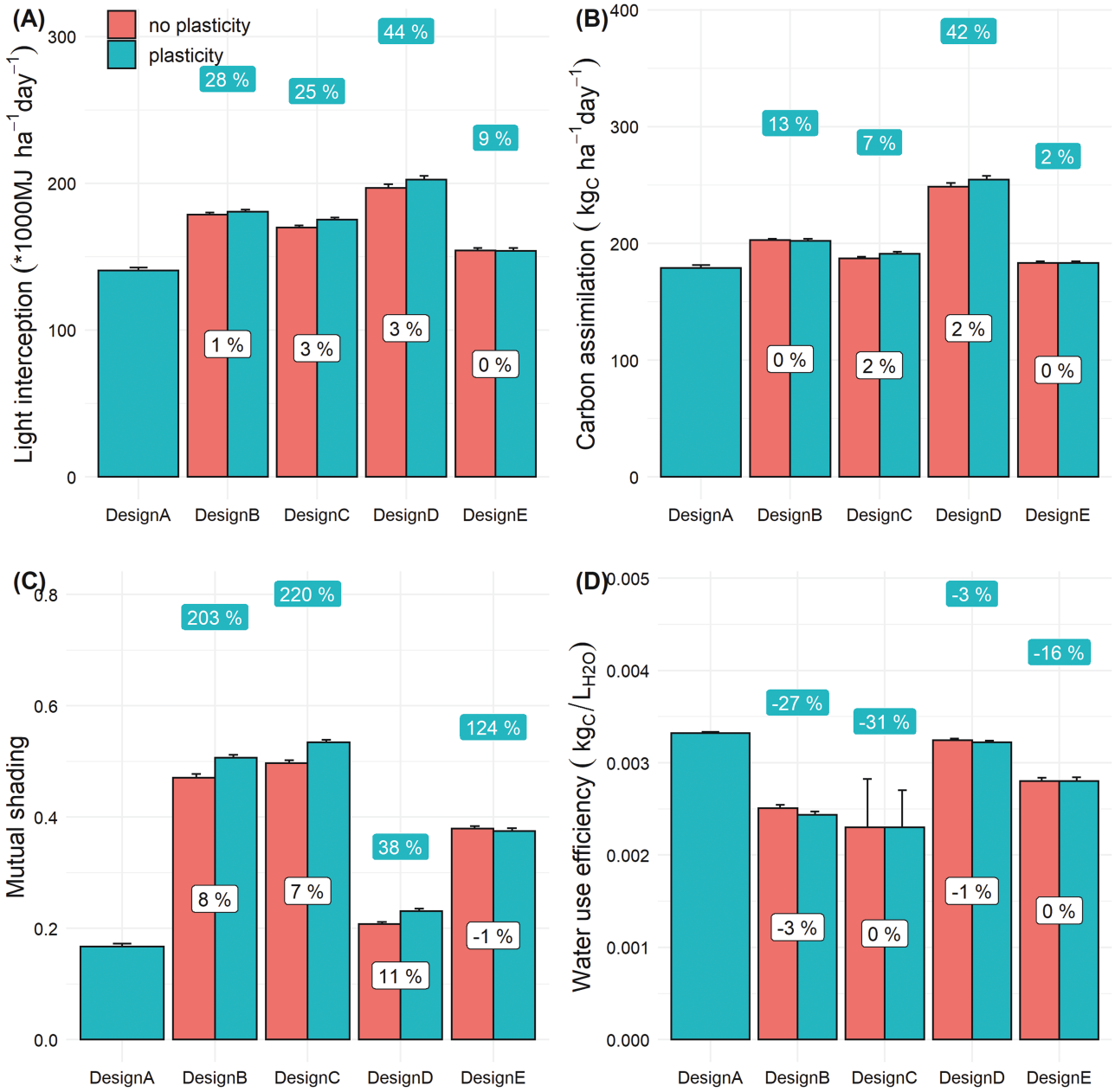

Figure 8. Simulation outputs at the stand scale for each design using plastic responses in the model (blue boxes) or not (red boxes). Bars indicate the mean value and error bars the standard deviation of the seven simulations. Values in blue labels on top of bars represent inter-design comparison, i.e. gain or loss relatively to the design control (design A). Values in white labels on bars represent the gain or loss when architectural plasticity is considered in simulations.

Pallas *et al.* (2013a) demonstrated how source–sink imbalance could modulate yield components. As a result, it is likely that the cost of allocating additional biomass in leaf expansion will be at the expense of bunch production. Comparison of the designs in term of oil production would be very interesting to investigate whether the estimated improvement in total carbon assimilation at the plot scale for some designs involved increasing yield or not.

Eventually, the coupling between the structural model VPalm and the carbon assimilation model XPalm developed by Pallas (Pallas *et al.* 2013b) would enable to predict oil palm yield performance depending on planting designs. Such development would also enable to take into account the root system in the model and would consider competition for water, which was neglected in the present work.

5. CONCLUSION

The present study supports the value of using FSPMs in an agronomic context. *In silico* experiments estimated the importance of architectural plasticity in physiological processes, and drew attention

to the physiological consequences of the limited architectural plasticity of oil palm when planting designs are inappropriate. Indeed, the leaf expansion in response to shade together with the inability of oil palm to modulate mutual shading decreased carbon assimilation at the stand scale. The modelling tool presented here paves the way to design innovative patterns of plantation based on *in silico* estimations of plant performance. Architectural screening of an enlarged diversity of oil palm architecture, involving *E. oleifera* × *E. guineensis* hybrids which present shorter leaves (Barcelos *et al.* 2015), could extend the possibility of defining planting designs specific to genetic material. Furthermore, in the context of rising interest for 'ecologically intensified' oil palm systems (Bhagwat and Willis 2008; Khasanah *et al.* 2020), the modelling approach proposed in this paper will help providing insights in the comprehension of the ecophysiological processes driving performance of oil palm agroforestry and intercropping systems.

SUPPORTING INFORMATION

The following additional information is available in the online version of this article—

Figure S1. Description of planting patterns and neighbourhood.

Table S1. Analysis of covariance table of rachis length to assess the effect of plots.

Figure S2. Rachis length depending on leaf rank for the five studied designs and the two plots.

Figure S3. Description of the leaf and the remarkable points.

Appendix S1. Estimation of the shear modulus.

Figure S4. Mechanical device used to estimate the shear modulus (G) of the rachis.

Figure S5. Optimization process to adjust the modulus of elasticity (E).

Figure S6. Correlations between the selected NI (minimal distance between plants) and the others neighbourhood indices tested to design allometries.

Figure S7. Leaf bending depending on manual versus LiDAR-based measurements.

Figure S8. Mock-ups generated with the VPalm model for each design.

Table S2. Coefficient of variation of variable outputs estimated from the seven simulations on each design.

ACKNOWLEDGEMENTS

The authors make special thanks to the SMARTRI staff for the logistic and technical assistance for their much valued help in the field data acquisition. The authors are also grateful for the comments of the three anonymous reviewers, and particularly reviewer 1 for his inputs on statistical revisions.

SOURCES OF FUNDING

This work was financially supported by the SMART Research Institute (SMARTRI, Smart Tbk.).

CONFLICT OF INTEREST

None declared.

CONTRIBUTIONS BY THE AUTHORS

Conceptualization: R.P.A.P., R.V., J.-P.C. and J.D.; software and methodology: R.P.A.P., R.V., J.D., L.B., F.G. and F.B.; data analysis: R.P.A.P., R.V., L.B. and D.A.R.; investigation: R.P.A.P., R.V., J.D. and J.-P.C.; resources: D.A.R. and J.-P.C.; data curation: R.P.A.P., R.V., M.R. and D.A.R.; writing—original draft preparation: R.P.A.P.; writing—review and editing: R.P.A.P., R.V., L.B., F.B., D.A.R. and J.-P.C.; visualization: R.P.A.P., R.V., M.R., and F.B.; supervision: R.P.A.P. and R.V.; project administration: R.P.A.P., R.V., D.A.R. and J.-P.C.

DATA AVAILABILITY

Processed data, as well as models code, are available from the authors upon request. Archimed-phi model is available online (https://archimed-platform.github.io/archimed-phys-user-doc/). An example configuration of simulation is available in Zenodo repository (doi:10.5281/zenodo.6246090).

LITERATURE CITED

Aphalo PJ, Ballare CL, Scopel AL. 1999. Plant–plant signalling, the shade-avoidance response and competition. *Journal of Experimental Botany* **50**:1629–1634.

Assefa Y, Carter P, Hinds M, Bhalla G, Schon R, Jeschke M, Paszkiewicz S, Smith S, Ciampitti IA. 2018. Analysis of long term study indicates both agronomic optimal plant density and increase maize yield per plant contributed to yield gain. *Scientific Reports* **8**:1–11.

Ballaré CL, Pierik R. 2017. The shade-avoidance syndrome: multiple signals and ecological consequences. *Plant, Cell & Environment* **40**:2530–2543.

Ballaré CL, Scopel AL, Sánchez RA. 1990. Far-red radiation reflected from adjacent leaves: an early signal of competition in plant canopies. *Science* **247**:329–332.

Barcelos E, Rios S de A, Cunha RNV, Lopes R, Motoike SY, Babiychuk E, Skirycz A, Kushnir S. 2015. Oil palm natural diversity and the potential for yield improvement. *Frontiers in Plant Science* **6**:190.

Barillot R, Escobar-Gutiérrez AJ, Fournier C, Huynh P, Combes D. 2014. Assessing the effects of architectural variations on light partitioning within virtual wheat–pea mixtures. *Annals of Botany* **114**:725–737.

Bhagwat SA, Willis KJ. 2008. Agroforestry as a solution to the oil-palm debate. *Conservation Biology* **22**:1368–1369.

Bongers FJ, Pierik R, Anten NPR, Evers JB. 2018. Subtle variation in shade avoidance responses may have profound consequences for plant competitiveness. *Annals of Botany* **121**:863–873.

Bonneau X, Impens R, Buabeng M. 2018. Optimum oil palm planting density in West Africa. *OCL - Oilseeds and fats, crops and lipids* **25**:A201.

Bonneau X, Vandessel P, Buabeng M, Erhahuyi C. 2014. Early impact of oil palm planting density on vegetative and oil yield variables in West Africa. *Agronomy* **21**:0–6.

Boudon F, Preuksakarn C, Ferraro P, Diener J, Nacry P, Nikinmaa E, Godin C. 2014. Quantitative assessment of automatic reconstructions of branching systems obtained from laser scanning. *Annals of Botany* **114**:853–862.

Buck-Sorlin G, De Visser PHB, Henke M, Sarlikioti V, Van Der Heijden GWAM, Marcelis LFM, Vos J. 2011. Towards a

functional–structural plant model of cut-rose: simulation of light environment, light absorption, photosynthesis and interference with the plant structure. *Annals of Botany* **108**:1121–1134.

Chelle M, Evers JB, Combes D, Varlet-Grancher C, Vos J, Andrieu B. 2007. Simulation of the three-dimensional distribution of the red:far-red ratio within crop canopies. *New Phytologist* **176**:223–234.

Dauzat J, Rapidel B, Berger A. 2001. Simulation of leaf transpiration and sap flow in virtual plants: model description and application to a coffee plantation in Costa Rica. *Agricultural and Forest Meteorology* **109**:143–160.

Demotes-Mainard S, Péron T, Corot A, Bertheloot J, Le Gourrierec J, Pelleschi-Travier S, Crespel L, Morel P, Huché-Thélier L, Boumaza R, Vian A, Guérin V, Leduc N, Sakr S. 2016. Plant responses to red and far-red lights, applications in horticulture. *Environmental and Experimental Botany* **121**:4–21.

Duursma RA, Falster DS, Valladares F, Sterck FJ, Pearcy RW, Lusk CH, Sendall KM, Nordenstahl M, Houter NC, Atwell BJ, Kelly N, Kelly JWG, Liberloo M, Tissue DT, Medlyn BE, Ellsworth DS. 2012. Light interception efficiency explained by two simple variables: a test using a diversity of small- to medium-sized woody plants. *New Phytologist* **193**:397–408.

Evers JB, Vos J, Chelle M, Andrieu B, Fournier C, Struik PC. 2007. Simulating the effects of localized red: far-red ratio on tillering in spring wheat (*Triticum aestivum*) using a three-dimensional virtual plant model. *New Phytologist* **176**:325–336.

Evers JB, Bastiaans L. 2016. Quantifying the effect of crop spatial arrangement on weed suppression using functional–structural plant modelling. *Journal of Plant Research* **129**:339–351.

Farquhar GD, Caemmerer S, Berry JA. 1980. A biochemical model of photosynthetic CO_2 assimilation in leaves of C_3 species. *Planta* **149**:78–90.

Franklin KA. 2008. Shade avoidance. *New Phytologist* **179**:930–944.

Furbank RT, Jimenez-Berni JA, George-Jaeggli B, Potgieter AB, Deery DM. 2019. Field crop phenomics: enabling breeding for radiation use efficiency and biomass in cereal crops. *New Phytologist* **223**:1714–1727.

Gommers CMM, Visser EJW, Onge KRS, Voesenek LACJ, Pierik R. 2013. Shade tolerance: when growing tall is not an option. *Trends in Plant Science* **18**:65–71.

Kahlen K, Stützel H. 2011. Modelling photo-modulated internode elongation in growing glasshouse cucumber canopies. *New Phytologist* **190**:697–708.

Khasanah N, van Noordwijk M, Slingerland M, Sofiyudin M, Stomph D, Migeon AF, Hairiah K. 2020. Oil palm agroforestry can achieve economic and environmental gains as indicated by multifunctional land equivalent ratios. *Frontiers in Sustainable Food Systems* **3**:1–13.

Kush GS. 2001. Green revolution: the way forward. *Nature Reviews Genetics* **2**:815–822.

Lagarias JC, Reeds JA, Wright MH, Wright PE. 1998. Convergence properties of the Nelder–Mead simplex method in low dimensions. *SIAM Journal on Optimization* **9**:112–147.

Lamanda N, Dauzat J, Jourdan C, Martin P, Malézieux E. 2008. Using 3D architectural models to assess light availability and root bulkiness in coconut agroforestry systems. *Agroforestry Systems* **72**:63–74.

Lecarpentier C, Barillot R, Blanc E, Abichou M, Goldringer I, Barbillon P, Enjalbert J, Andrieu B. 2019. Walter: a three-dimensional wheat model to study competition for light through the prediction of tillering dynamics. *Annals of Botany* **123**:961–975.

Legros S, Mialet-Serra I, Caliman JP, Siregar FA, Clement-Vidal A, Fabre D, Dingkuhn M. 2009. Phenology, growth and physiological adjustments of oil palm (*Elaeis guineensis*) to sink limitation induced by fruit pruning. *Annals of Botany* **104**:1183–1194.

Lin Y. 2015. LiDAR: an important tool for next-generation phenotyping technology of high potential for plant phenomics? *Computers and Electronics in Agriculture* **119**:61–73.

Louarn G, Da Silva D, Godin C, Combes D. 2012. Simple envelope-based reconstruction methods can infer light partitioning among individual plants in sparse and dense herbaceous canopies. *Agricultural and Forest Meteorology* **166–167**:98–112.

Medlyn BE, Duursma RA, Eamus D, Ellsworth DS, Prentice IC, Barton CVM, Crous KY, De Angelis P, Freeman M, Wingate L. 2011. Reconciling the optimal and empirical approaches to modelling stomatal conductance. *Global Change Biology* **17**:2134–2144.

Monteith JL, Unsworth MH. 2008. Steady-state heat balance: water surfaces, soil, and vegetation. I. In: *Principles of environmental physics*, 3rd edn. London: Elsevier; 229–257.

Munier-Jolain NM, Guyot SHM, Colbach N. 2013. A 3D model for light interception in heterogeneous crop: weed canopies: model structure and evaluation. *Ecological Modelling* **250**:101–110.

Nelder JA, Mead R. 1965. A simplex method for function minimization. *The Computer Journal* **7**:308–313.

Pallas B, Mialet-Serra I, Rouan L, Clément-Vidal A, Caliman JP, Dingkuhn M. 2013a. Effect of source/sink ratios on yield components, growth dynamics and structural characteristics of oil palm (*Elaeis guineensis*) bunches. *Tree Physiology* **33**:409–424.

Pallas B, Soulié JC, Aguilar G, Rouan L, Luquet D. 2013b. X-Palm, a functional structural plant model for analysing temporal, genotypic and inter-tree variability of oil palm growth and yield. In *International Conference on Functional Structure Plant Models*. Finnish Society of Forest Science.

Perez RPA. 2017. Analyzing and modelling the genetic variablility of aerial architecture and light interception of the oil palm (*Elaeis guineensis* Jacq). Doctoral dissertation, Montpellier, SupAgro.

Perez RPA, Dauzat J, Pallas B, Lamour J, Verley P, Caliman JP, Costes E, Faivre R. 2018. Designing oil palm architectural ideotypes for optimal light interception and carbon assimilation through a sensitivity analysis of leaf traits. *Annals of Botany* **121**:909–926.

Perez RP, Fournier C, Cabrera-Bosquet L, Artzet S, Pradal C, Brichet N, Chen TW, Chapuis R, Welcker C, Tardieu F. 2019. Changes in the vertical distribution of leaf area enhanced light interception efficiency in maize over generations of selection. *Plant, Cell & Environment* **42**:2105–2119.

Perez RPA, Pallas B, Le Moguédec G, Rey H, Griffon S, Caliman J-P, Costes E, Dauzat J. 2016. Integrating mixed-effect models into an architectural plant model to simulate inter- and intra-progeny variability: a case study on oil palm (*Elaeis guineensis* Jacq.). *Journal of Experimental Botany* **67**:4507–4521.

Perez RPA, Vezy R, Brancheriau L, Boudon F, Grand F, Raharjo DA, Caliman J-P, Dauzat J. 2022. ARCHIMED-φ simulation files for the simulation of design A from the article "When architectural plasticity fails to counter the light competition imposed by planting

design: an *in silico* approach using a functional–structural model of oil palm." Zenodo: doi:10.5281/ZENODO.6246090.

Pierik R, De Wit M. 2014. Shade avoidance: phytochrome signalling and other aboveground neighbour detection cues. *Journal of Experimental Botany* **65**:2815–2824.

Pierik R, Testerink C. 2014. The art of being flexible: how to escape from shade, salt, and drought. *Plant Physiology* **166**:5–22.

Rafii MY, Isa ZA, Kushairi A, Saleh GB, Latif MA. 2013. Variation in yield components and vegetative traits in Malaysian oil palm (*Elaeis guineensis* Jacq.) *dura* × *pisifera* hybrids under various planting densities. *Industrial Crops and Products* **46**:147–157.

Reynolds M.P., van Ginkel M. & Ribaut J.M. 2000. Avenues for genetic modification of radiation use efficiency in wheat. *Journal of Experimental Botany* **51**:459–473.

Sarlikioti V, De Visser PHB, Buck-Sorlin GH, Marcelis LFM. 2011. How plant architecture affects light absorption and photosynthesis in tomato: towards an ideotype for plant architecture using a functionalstructural plant model. *Annals of Botany* **108**:1065–1073.

Da Silva D, Han L, Faivre R, Costes E. 2014. Influence of the variation of geometrical and topological traits on light interception efficiency of apple trees: sensitivity analysis and metamodelling for ideotype definition. *Annals of Botany* **114**:739–752.

Thapa S, Zhu F, Walia H, Yu H, Ge Y. 2018. A novel LiDAR-Based instrument for high-throughput, 3D measurement of morphological traits in maize and sorghum. *Sensors (Switzerland)* **18**:1187.

Truong SK, McCormick RF, Rooney WL, Mullet JE. 2015. Harnessing genetic variation in leaf angle to increase productivity of *Sorghum bicolor*. *Genetics* **201**:1229–1238.

Valladares F, Gianoli E, Gómez JM. 2007. Ecological limits to plant phenotypic plasticity. *New Phytologist* **176**:749–763.

Vos J, Evers JB, Buck-Sorlin GH, Andrieu B, Chelle M, De Visser PHB. 2010. Functional–structural plant modelling: a new versatile tool in crop science. *Journal of Experimental Botany* **61**:2101–2115.

Willaume M, Lauri PE, Sinoquet H. 2004. Light interception in apple trees influenced by canopy architecture manipulation. *Trees - Structure and Function* **18**:705–713.

Zhu J, van der Werf W, Anten NPR, Vos J, Evers JB. 2015. The contribution of phenotypic plasticity to complementary light capture in plant mixtures. *New Phytologist* **207**:1213–1222.

Ziamtsov I, Navlakha S. 2019. Machine learning approaches to improve three basic plant phenotyping tasks using three-dimensional point clouds. *Plant Physiology* **181**:1425–1440.